The Journal of Chemical Physics

Theoretical study on L–H^+–L with identical donors: Short strong hydrogen bond or not?

Cite as: J. Chem. Phys. **157**, 094302 (2022); https://doi.org/10.1063/5.0103228
Submitted: 14 June 2022 • Accepted: 05 August 2022 • Accepted Manuscript Online: 08 August 2022 • Published Online: 06 September 2022

Wanwan Feng (丰琬琬), Dan Li (李丹) and Longjiu Cheng (程龙玖)

The Journal of Chemical Physics ARTICLE scitation.org/journal/jcp

Theoretical study on L–H$^+$–L with identical donors: Short strong hydrogen bond or not?

Cite as: J. Chem. Phys. 157, 094302 (2022); doi: 10.1063/5.0103228
Submitted: 14 June 2022 • Accepted: 5 August 2022 •
Published Online: 6 September 2022

Wanwan Feng (丰婉婉),[1] Dan Li (李丹),[1,a)] and Longjiu Cheng (程龙玖)[1,2,a)]

AFFILIATIONS

[1] Department of Chemistry, Anhui University, 111 Jiulong Road, Hefei, Anhui 230601, China
[2] Laboratory of Structure and Functional Regulation of Hybrid Materials, Ministry of Education, Anhui University, Hefei 230601, People's Republic of China

[a)] **Authors to whom correspondence should be addressed:** ahulidan@aliyun.com and clj@ustc.edu

ABSTRACT

Short strong hydrogen bonds (SSHBs) play a crucial role in many chemical processes. Recently, as the representative of SSHBs, [F–H–F]$^-$ was experimentally observed. [F–H–F]$^-$ has a symmetric structure, which can be described as a H$^+$ acid shared by two terminal F$^-$ donors (F$^-$–H$^+$–F$^-$). To explore whether two identical donors are bound to result in SSHBs, we performed theoretical studies on a series of compounds (L–H$^+$–L) with two identical electron donors (L corresponds to donors containing group 14, 15, 16, and 17 elements). The results show that identical donors do not definitely lead to SSHBs. Instead, typical hydrogen bonds also exist. Both electronegativity and basicity contribute to the patterns of hydrogen bonds, where more electronegative and weaker donors benefit to SSHBs. In addition, it was found that zero-point energies also respond to the hydrogen bonding systems. This systemic work is expected to provide more insights into SSHBs.

I. INTRODUCTION

Hydrogen bond (HB) has been a hot research topic since it was first described by Latimer and Rodebush in 1920.[1–5] It plays important roles in chemistry, biology, and material sciences,[6–10] participating in crystal engineering[11–14] and supramolecular chemistry.[15–19] It is conventionally expressed as D–H···A, where D is HB donor, while A is HB acceptor.[20–23] The distance between proton and acceptor atoms (H···A) is usually shorter than the sum of their van der Waals radii,[24] but this may not hold in weaker hydrogen bond systems.[25,26]

It is well known that the strength of HBs varies over a wide range, and they could be too weak to distinguish them from van der Waals interactions or as strong as a covalent bond.[26,27] Typical HBs mainly possess weak or moderate strength. In contrast, short strong hydrogen bonds (SSHBs), which play a crucial role in transition-state stabilization in enzymatic catalysis,[28–31] have a relatively great strength of roughly 15–40 kcal/mol.[32] Besides great strengths, SSHBs are conventionally characterized by very short donor–acceptor distances, high frequency ^{1}H NMR signals, and intense continuous IR absorption.[33]

The nature of typical weak HB is mainly ascribed to electrostatic interaction,[34–36] protons strongly bond with the HB donor, leaving the other segment a weak interaction. Nevertheless, SSHBs are thought to be covalent in nature, which are always taken as a result of a three-center four-electron (3c–4e) interaction.[37–39] In typical HBs, hydrogen transfer between the donors and acceptors is difficult,[29,40,41] whereas protons in SSHBs are shared by donors and acceptors. From the perspective of a potential energy scan, SSHBs are also called low-barrier hydrogen bonds (LBHBs) since they correspond to systems having single-well with no barrier or double-well with a low barrier for the proton transfer process between the donor and acceptor atoms.[41–44]

Recently, as the representative of SSHB, [F–H–F]$^-$ was experimentally observed by Dereka *et al.*[45] [F–H–F]$^-$[46,47] has a symmetric structure, which can be described as a H$^+$ acid shared by two terminal F$^-$ donors (F$^-$–H$^+$–F$^-$). In terms of the requirements for forming SSHBs, the probably universally accepted criterion is the pK_a/PA (proton affinity) matched principle.[48,49] It states that HB strength increases with the decreasing ΔpK_a or ΔPA, where $\Delta pK_a = pK_a(D–H) - pK_a(A–H^+)$ and $\Delta PA = P(D^-) - P(A)$, and the strength reaches a maximum when $\Delta pK_a/\Delta PA$ approaches zero.[26] Obviously, [F–H–F]$^-$ satisfies the principle with identical donors. In this work, to explore whether two identical donors are bound to result in SSHBs, we carried out a theoretical study on a series of species composed of H$^+$ and two ligands (L–H$^+$–L,

where L corresponds to donors containing group 14, 15, 16, and 17 elements). Though several cases with identical groups were reported,[29,50–52] it deserves systemic and deep study. It was found that most complexes also exhibited characteristics similar to that of $[F–H–F]^-$, forming SSHBs, while others possessed typical HBs. The electronegativity and basicity were discussed, and the results can further deepen our understanding of SSHBs.

II. COMPUTATIONAL METHODS

To confirm the computational method for our system, we performed calculations under several density functional theory (DFT), second-order Møller–Plesset (MP2),[53] and coupled cluster with single, double, and perturbative triple excitations [CCSD(T)][54] theory levels to compare the values of the bond lengths and frequencies with the corresponding experimental results of $[F–H–F]^-$. As shown in Table S1, the H–F bond length and binding energy of $[F–H–F]^-$ at the MP2/def2-QZVP level were close to the experimental values.[55] Furthermore, we performed potential energy surface (PES) for $[F–H–F]^-$ using different methods, as shown in Figs. S1 and S2, of the supplementary material and the results obtained by MP2/def2-QZVP were the closest to that of CCSD(T). Therefore, MP2/def2-QZVP was considered appropriate for structural optimization and PES.

All the geometries in this work were optimized at MP2/def2-QZVP level and frequencies were checked without false frequencies. In addition, PESs were performed at the same theoretical level. Chemical bonding analysis was carried out at M06-2X[56]/def2-TZVPP level of theory with MP2-optimized structures by using the adaptive natural density partitioning (AdNDP)[57] method. AdNDP allows an electron pair to be delocalized over n atoms with n ranging from one to the total number of atoms in the whole molecule. This method accepts only those bonding elements whose occupation numbers (ON) exceed the specified threshold values, which are usually chosen to be close to 2.00 |e|. Noncovalent interaction (NCI) analyses[58] were carried out, and the results were shown in the scatter plots of the reduced density gradient (RDG) vs the electron density (ρ) multiplied by the sign of λ_2 [sign(λ_2)ρ]. The electron densities of the compounds were analyzed by electron localization function (ELF)[59] and localized orbital locator (LOL).[60] The calculation of the binding energy of the complexes includes basis set superposition error (BSSE)[61] corrections ($E_b = E + E_{BSSE}$) and was referenced to the optimized geometries of the fragments that compose the molecule. BSSE is commonly removed or reduced by using the counterpoise correction, which was developed by Boys and Bernardi.[62]

Energy decomposition analysis was performed by the symmetry-adapted perturbation theory (SAPT)[63] at the SAPT2+(3) δMP2/def2-QZVP level. The intermolecular interaction energy (E_{int}) was performed using SAPT to decompose the total interaction energy (E_{int}) into

$$E_{int} = E_{elst} + E_{exch} + E_{ind} + E_{disp},$$

where E_{elst} is the classical Coulomb interaction, E_{exch} defines the exchange-repulsion term, and E_{ind} represents the energy of interaction of the permanent multipole moments of one monomer and the induced multipole moments of the other. This term is interpreted as orbital interaction, representing the polarization of the electron density between monomers, E_{disp} is the dispersion interaction energy. The value of pK_b indicates the strength of the basicity of L, $pK_b = -\lg[\exp(-\Delta G/RT)]$, where $\Delta G = G(H^+–L) – G(H^+) – G(L)$.

All the calculations were carried out in the Gaussian16 package.[64] NCI, ELF, and LOL analyses were completed with the Multiwfn[65] tool. Molecular visualization was performed using the MOLEKEL 5.4 software.[66] Energy decomposition analysis was performed on PSI4 package.[67]

III. RESULTS AND DISCUSSION

$[F–H–F]^-$, as the representative of SSHBs, satisfies the pK_a/PA matched principle with two identical donors. It can be described by the Lewis theory model with the middle H^+ cation serving as the Lewis acid and two terminal F^- anions acting as the Lewis base. Based on the structure of $[F–H–F]^-$, we chose a series of electron donors L (L = F^-, Cl^-, Br^-, I^-, HF, HCl, HBr, HI, OH^-, HS^-, HSe^-, HTe^-, H_2O, H_2S, H_2Se, H_2Te, NH_2^-, PH_2^-, AsH_2^-, SbH_2^-, NH_3, PH_3, AsH_3, SbH_3, CH_3^-, CF_3^-, $H_4N_2C_3$, and CCH^-, respectively) to interact with H^+ to explore whether two identical donors definitely result in symmetric SSHBs.

A. Structural and electronic properties of $[F–H–F]^-$

First, we focus on the property of $[F–H–F]^-$, as shown in Fig. 1, we scanned the PES of $[F–H–F]^-$ as a function of the distances of $F_1\cdots H$ (r_1) and $H\cdots F_2$ (r_2), where the F–H bond length in HF monomer (r_0 = 0.92 Å) is taken as the unit length. Clearly, there is one minimum on the PES, and the most stable structure has two equal H···F lengths of 1.14 Å (r_1/r_0 = 1.24, structure **I**). The black dash line can be seen as the dissociation pathway of $[F–H–F]^-$ to $F^-\cdots H–F$, and we chose structures **II** ($F_1\cdots H$ = 1.54 Å, r_1/r_0 = 1.67) and **III** ($F_1\cdots H$ = 1.94 Å, r_1/r_0 = 2.11) to investigate the evolution of HB, where structures **I** is SSHB, **III** is typical HB, and **II** is an intermediate state.

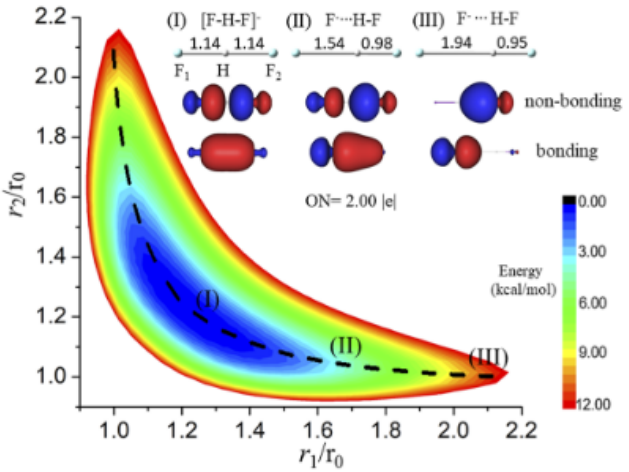

FIG. 1. PES of $[F–H–F]^-$, bonding and non-bonding orbitals of structures **I**, **II**, and **III** (as labeled) by the AdNDP analyses based on 3c–4e model, where r_1, r_2, and r_0 represent $F_1\cdots H$ distance, $H\cdots F_2$ distance, and the bond length of the HF monomer. All the distances are given in Å.

To investigate the chemical bonding patterns of short strong and typical HBs, we performed the AdNDP analyses of structures **I**, **II**, and **III**, which is also plotted in Fig. 1. Obviously, the structure **I** can be well described by two symmetric 3c–2e bonds with idealized occupation numbers (2.00 |e|), corresponding to bonding and non-bonding bonds, respectively. When the length of $F_1\cdots H$ is fixed at 1.54 Å, $H\cdots F_2$ distance is shortened to 0.98 Å (structure **II**). It can also be described by 3c–4e bonds. However, different from the structure **I**, the bonding orbital shifts to F_1 and the non-bonding orbital shift to F_2. Thus, 3c–4e bond of structure **II** is polarized. Moreover, when the $F_1\cdots H$ distance is further elongated to 1.94 Å (structure **III**), the 3c–4e bond is totally polarized to lone pairs of F_1 and σ-HF_2. Therefore, there is no clear boundary between short strong and typical HBs, and both of them can be ascribed to 3c–4e bond (equivalent or polarized), just like that in a halogen bond.[68] In addition, from the perspective of classical HB theory, HBs arise from electrostatic interactions. The electrostatic potential surface[69] of HF (Fig. S3) indeed shows a distinct σ-hole[70] that leads to strong interaction with F^-, forming $[F\text{–}H\text{–}F]^-$.

B. Structural and electronic properties of L–H$^+$–L

We further investigated the cases of L–H$^+$–L (L = F^-, Cl^-, Br^-, and I^-), the optimized structures and PESs were shown in Fig. 2(a). The structure information and the H$^+$–L bond lengths of HL monomers (r_0) are list in Table S2. PESs analyses show that compounds with Cl^-, Br^-, and I^- as ligands exhibit similar performance to that of $[F\text{–}H\text{–}F]^-$, structures in low energy (blue) concentrating on the central regions. In addition, as plotted in Fig. 2(b), the results of cases with neutral ligands (L = HF, HCl, HBr, and HI) are also similar. The potential energy curves in Figs. 2(c) and 2(d) clearly show that in the case of compounds with both anion and neutral groups as ligands, all the curves have single-well potentials,[51] indicating that besides $[F\text{–}H\text{–}F]^-$ other L–H$^+$–L (L = Cl^-, Br^-, I^-, HF, HCl, HBr, and HI) compounds all have symmetric structures.

Chemical bonding analyses of L–H$^+$–L (L = F^-, Cl^-, Br^-, I^-, HF, HCl, HBr, and HI) in Fig. 3 show that these compounds can be well described by two symmetric bonding and non-bonding orbitals reliable occupation numbers (2.00 |e|), further confirming the

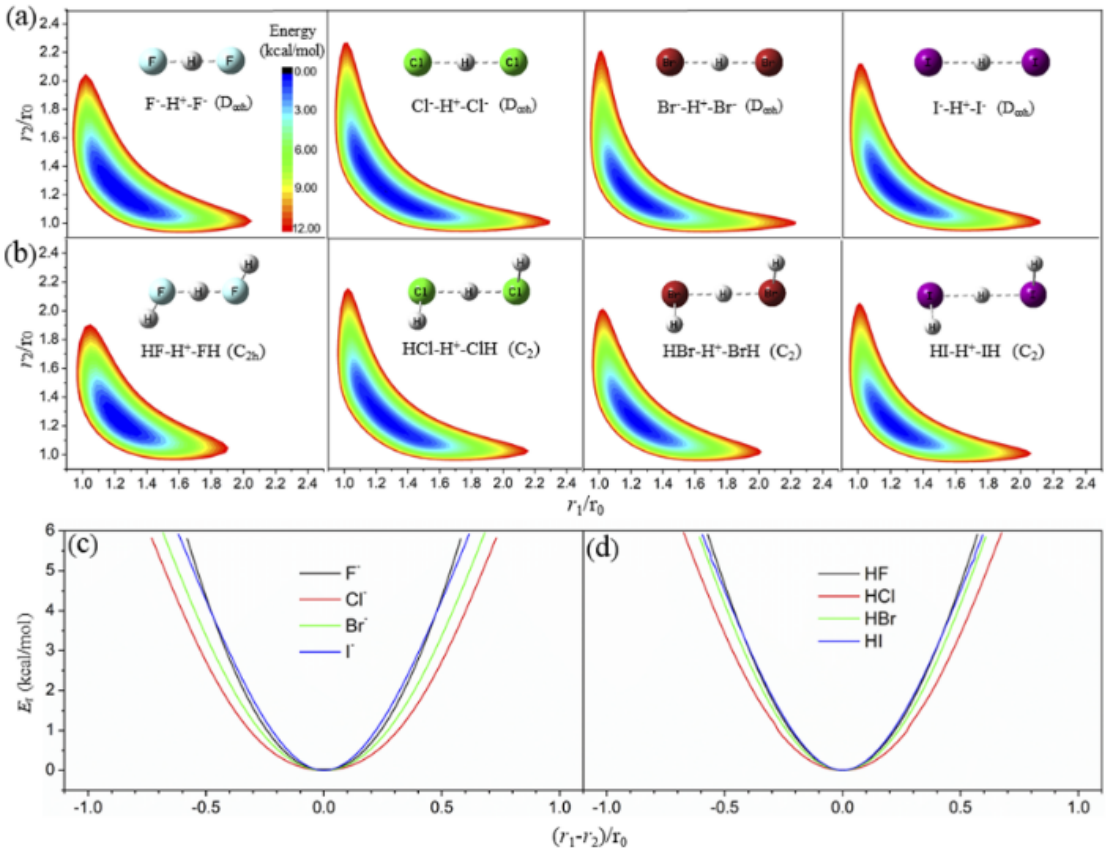

FIG. 2. Optimized structures and PESs of L–H$^+$–L with L = F^-, Cl^-, Br^-, and I^- (a); L = HF, HCl, HBr, and HI (b). Potential energy curves of L–H$^+$–L with L = F^-, Cl^-, Br^-, and I^- (c); L = HF, HCl, HBr, and HI (d). E_r is the relative energy of the dissociated and the most stable structures, r_1 and r_2 represent the lengths of two L–H$^+$ segments, respectively, and r_0 is the bond length of HL monomer.

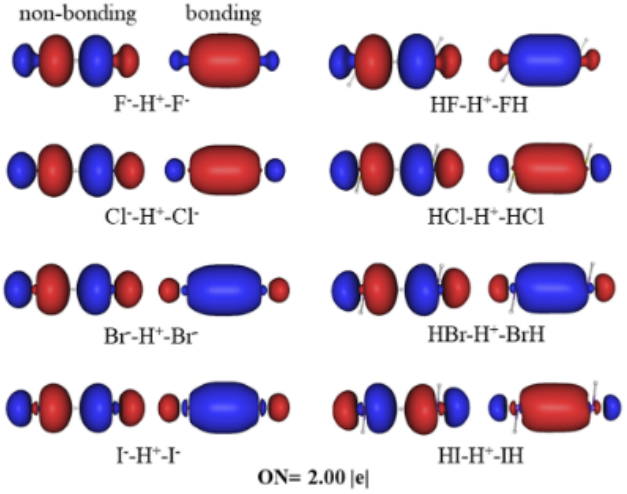

FIG. 3. Bonding (right) and non-bonding (left) 3c–2e orbitals of L–H^+–L (L = F^-, Cl^-, Br^-, I^-, HF, HCl, HBr, and HI) complexes by the AdNDP analyses.

existence of SSHBs. The results are in good agreement with those by PESs.

Moreover, analyses containing group 16 elements were carried out, Figs. 4(a) and 4(b) give the PESs of compounds with anion (OH^-, HS^-, HSe^-, and HTe^-) and neutral (H_2O, H_2S, H_2Se, and H_2Te) groups as donors, respectively. Similar to the results in Figs. 2(a) and 2(b), structures in low energy concentrate on the central regions. However, potential energy curves in Figs. 4(c) and 4(d) are somewhat different from those in Fig. 2. Curves in Figs. 4(c) and 4(d) are flatter, and it can be observed from the magnifying insets [Fig. 4(c)] that curves with L = OH^- and HS^- actually have double-well potentials, each having a low energy barrier. In contrast, the other curves have single-well potentials. Therefore, though two identical bases compete for H^+, compounds with HSe^-, HTe^- and neutral groups as donors feature single-well HBs, while HO^-–H^+–OH^- and HS^-–H^+–SH^- possess low barrier HBs. Chemical bonding analyses (Fig. S4) show that the bonding and non-bonding orbitals of HS^-–H^+–SH^- are polarized, other compounds can also be well described by two symmetric bonding and non-bonding orbitals with reliable occupation number (2.00 |e|). Though both HO^-–H^+–OH^- and HS^-–H^+–SH^- feature low barrier

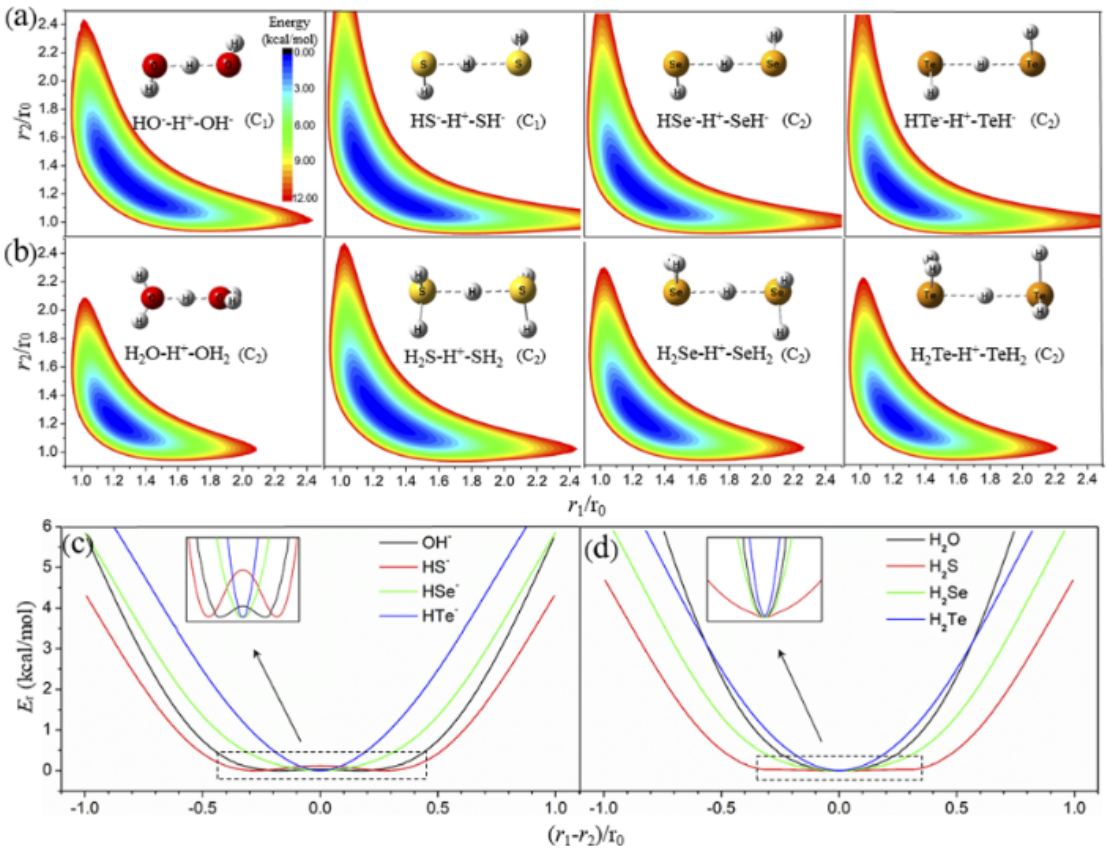

FIG. 4. Optimized structures and PESs of L–H^+–L with L = OH^-, HS^-, HSe^-, and HTe^- (a); L = H_2O, H_2S, H_2Se, and H_2Te (b). Potential energy curves of L–H^+–L with L = OH^-, HS^-, HSe^-, and HTe^- (c); L = H_2O, H_2S, H_2Se, and H_2Te (d). The insets in (c) and (d) show the magnification of the curves in the dotted boxes.

HBs, the polarization in orbitals of HO^-–H^+–OH^- is not as obvious as those of HS^-–H^+–SH^-, probably owing to the fairly low barrier of HO^-–H^+–OH^- for hydrogen transfer.

Furthermore, we extended the study to compounds containing group 15 elements. PESs of compounds with anion (NH_2^-, PH_2^-, AsH_2^-, and SbH_2^-, Fig. 5(a) and neutral [NH_3, PH_3, AsH_3, and SbH_3, Fig. 5(b)] groups as donors exhibit obvious difference from those in Figs. 2 and 4. When L = NH_2^-, PH_2^-, AsH_2^-, PH_3, AsH_3, and SbH_3, structures in low energy distributing in two parts. All the potential energy curves [Figs. 5(c) and 5(d)] have double-well potentials with obvious barriers, indicating that all these compounds possess typical or low barrier HBs. In addition, barriers increase in the order: PH_2^- > NH_2^- > AsH_2^- > SbH_2^- and PH_3 > AsH_3 > SbH_3 > NH_3. Note that the barriers of compounds containing phosphorus involve the highest barrier, indicating the particularity of phosphorus.[71] Unlike those of compounds containing group 16 and 17 elements, all the 3c–4e orbitals in Fig. S5 are polarized, just like F⁻···H–F.

Finally, as shown in Fig. S6, compounds containing carbon element (CH_3^-, CF_3^-, $H_4N_2C_3$, and CCH^-) were studied, and species containing other group 14 elements (Si, Ge, and Sn) preferred to form tetrel bonds[72–74] instead of HBs, which were not discussed here. Figure S6a indicates obvious asymmetric HBs for all these compounds, and the corresponding potential energy curves have very large barriers (Fig. S6b), suggesting typical HBs.

C. Effect of zero-point energy

Zero-point energy plays an important role in the transition between conventional and SSHBs.[45] Due to the particularly large number of structures on the PESs of the above systems, we selected seven species, namely L–H^+–L with L = F^-, OH^-, NH_2^-, PH_2^-, AsH_2^-, SbH_2^-, and CH_3^-, as representatives, to investigate the effect of zero-point energy. Zero-point energy of several dissociated structures with L = F^-, OH^-, NH_2^-, and CH_3^- [Fig. 6(a)] suggests that the zero-point energy of the symmetric structure ($r_1 = r_2$) is the lowest, and the zero-point energy of other dissociated structures is relative energy to the symmetric structure. The values of zero-point energy increase gradually with the increasing $|r_1-r_2|$ value and finally stabilizes, but the trend with L = F^- is the flattest. In addition, the difference in zero-point energy between the values of the symmetric structure and the stabilized values increases in the order

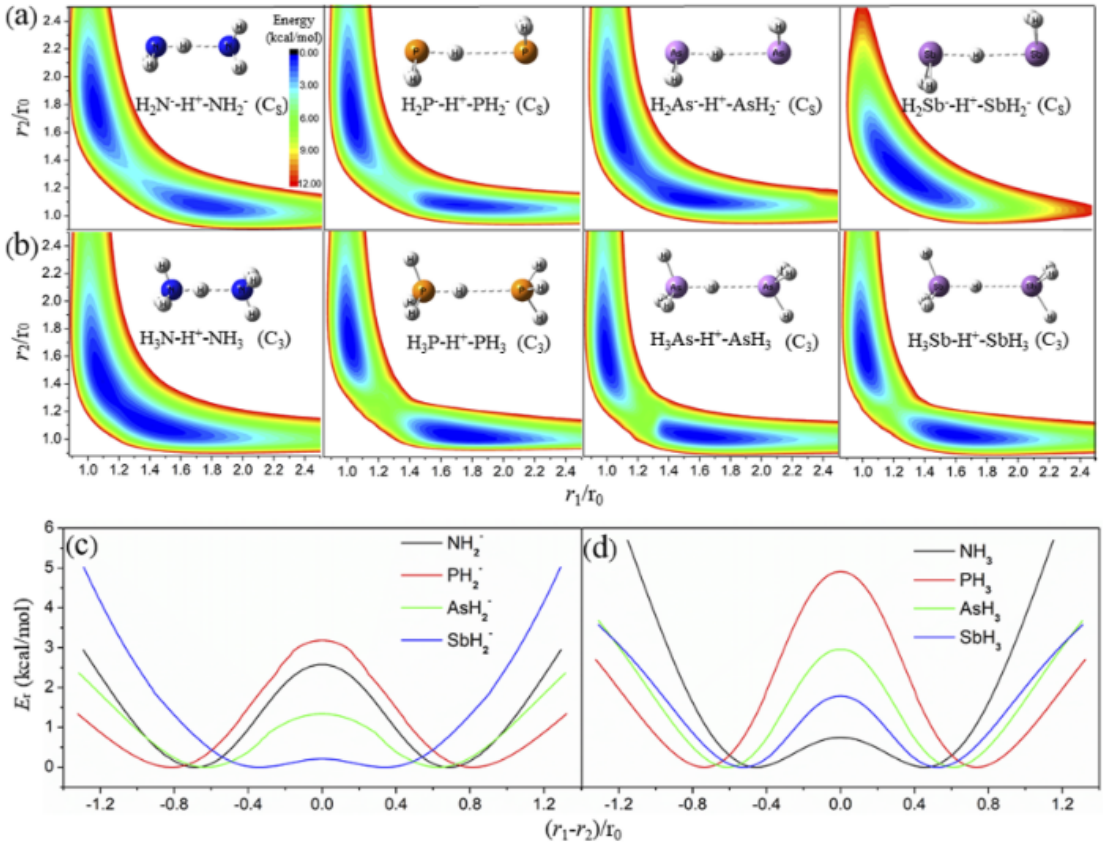

FIG. 5. Optimized structures and PESs of L–H^+–L with L = NH_2^-, PH_2^-, AsH_2^-, and SbH_2^- (a); L = NH_3, PH_3, AsH_3, and SbH_3 (b). Potential energy curves of L–H^+–L with L = NH_2^-, PH_2^-, AsH_2^-, and SbH_2^- (c); L = NH_3, PH_3, AsH_3, and SbH_3 (d).

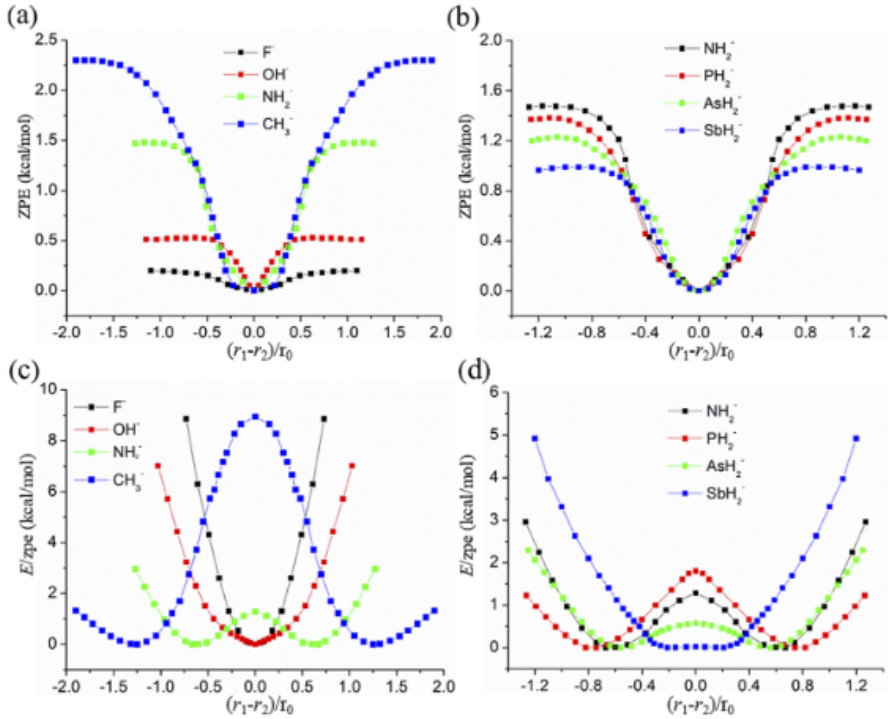

FIG. 6. The relative zero-point energy of L–H⁺–L with L = F⁻, OH⁻, NH_2^-, and CH_3^- (a); L = NH_2^-, PH_2^-, AsH_2^-, and SbH_2^- (b); potential energy curves of L–H⁺–L with L = F⁻, OH⁻, NH_2^-, and CH_3^- (c); L = NH_2^-, PH_2^-, AsH_2^-, and SbH_2^- (d), corrected by zero-point energy.

of $CH_3^- > NH_2^- > OH^- > F^-$. For compounds containing group 15 elements [Fig. 6(b)], the curves follow the same tendency, and the difference increases in the order of $NH_2^- > PH_2^- > AsH_2^- > SbH_2^-$. Then, we further explored the potential energy curves of these seven species considering zero-point energy. As plotted in Fig. 6(c), the curve of the compound with L = F⁻ still exhibits single-well potential, while that with L = OH⁻ changed from double-well [Fig. 4(c)] to single-well potential, the barrier disappearing. The structures with L = NH_2^- and CH_3^- still maintain double-well potential energy curves. For compounds with L = group 15 elements [Fig. 6(d)], all the curves still possess double-well potential, but the barriers become smaller compared with Fig. 5(d). Therefore, the potential energy curves are influenced by zero-point energy, but the main shape maintain except for structure with L = OH⁻. Zero-point energy plays a role in the forming of SSHBs, but it is not the main factor.

D. NCI, ELF, and LOL analyses

To further explore the properties of different types of HBs, NCI analyses of F⁻–H⁺–F⁻, HO⁻–H⁺–OH⁻, and H_3P–H⁺···PH_3 are compared [Fig. 7(a)]. One spike value at −0.18 indicates two equivalent strong interactions in F⁻–H⁺–F⁻. HO⁻–H⁺–OH⁻ has two close spikes at −0.18 and −0.14, respectively, indicating two comparable interactions in two H⁺–OH⁻ segments. In contrast, typical HB (H_3P–H⁺···PH_3) has two spikes at −0.18 and −0.03, respectively, suggesting that H⁺ strongly interacts with one of the PH_3 groups (−0.18), and the remaining H⁺···PH_3 segment is a weak interaction (−0.03). NCI analyses of other compounds are given in Figs. S7–S9.

Furthermore, Fig. 7(b) compares the ELF and LOL results of F⁻–H⁺–F⁻, HO⁻–H⁺–OH⁻, and H_3P–H⁺···PH_3, respectively. As expected, both ELF and LOL analyses show that F⁻–H⁺–F⁻ has equal forces on both sides of H⁺, while for HO⁻–H⁺–OH⁻ and H_3P–H⁺···PH_3 there are two different interactions within two H⁺–L segments and the difference in H_3P–H⁺···PH_3 is more apparent. ELF and LOL results agree well with NCI analyses. Moreover, ELF and LOL analyses for other complexes were also given in Figs. S10 and S11.

E. Energy decomposition analyses

To find out which effects play a more important role in the interaction energy, we selected seven complexes as representative for energy decomposition analyses, and the system was divided into two fragments (L–H⁺ and L). The energy contributions were summarized in Table S3, and E_{int} decreases in the order: F⁻–H⁺···F⁻ > HO⁻–H⁺···OH⁻ > Cl⁻–H⁺···Cl⁻ > Br⁻–H⁺···Br⁻ > I⁻–H⁺···I⁻ > H_2N^-–H⁺···NH_2^- > H_3C^-–H⁺···CH_3^-. To directly analyze the energy contributions, the percentage of the corresponding attractive terms (E_{elst}, E_{ind}, and E_{ind}) was plotted in Fig. S12. In general, E_{elst} and E_{ind} are the governing attractive forces. For the complexes with the same periodic elements (Fig. S12a), E_{ind} decreases from F⁻–H⁺···F⁻ to H_3C^-–H⁺···CH_3^-, and for typical HBs (H_2N^-–H⁺···NH_2^- and H_3C^-–H⁺···CH_3^-), E_{elst} is apparently stronger than E_{ind} and E_{disp}. Moreover, as depicted in Fig. S12b, for compounds containing group 17 elements, E_{elst} gradually decreases and E_{ind} increases from F⁻–H⁺···F⁻ to I⁻–H⁺···I⁻. In addition, both Figs. S12a and S12b show increases in the contribution of E_{disp}.

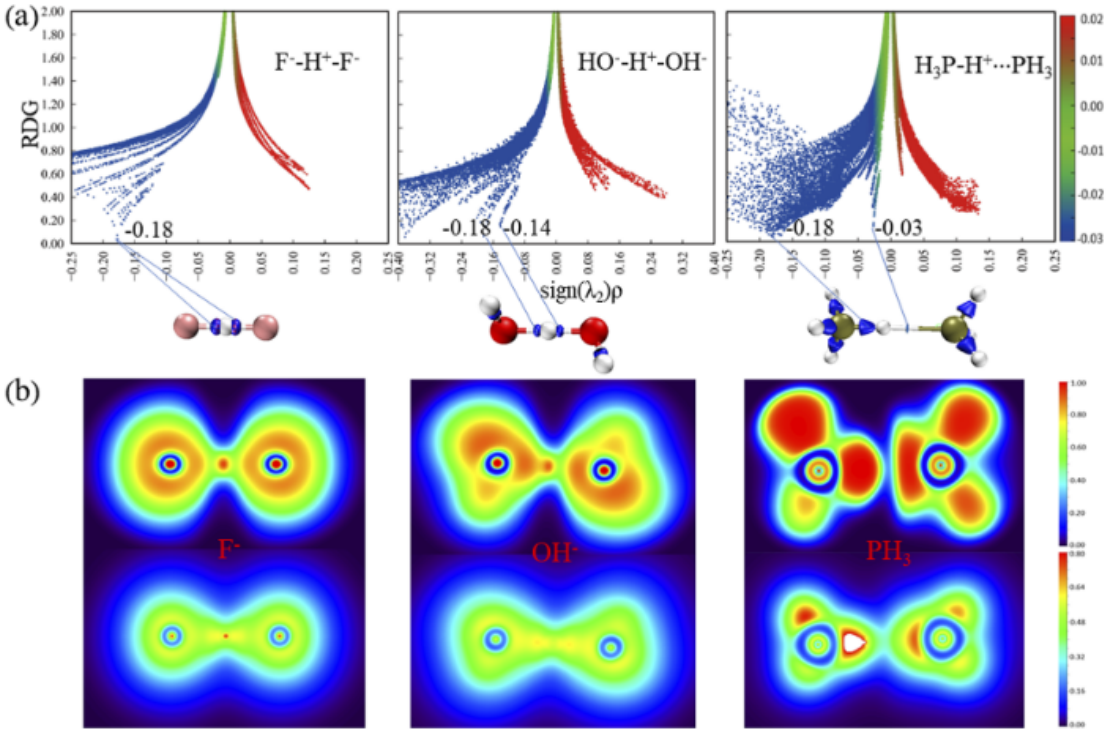

FIG. 7. (a) Plots of the reduced density gradient (RDG in a.u.) against the sign of the second Hessian eigenvalue multiplied by the electron density [sign(λ_2)ρ in a.u.] for F^-–H^+–F^-, HO^-–H^+–OH^-, and H_3P–$H^+\cdots PH_3$. (b) ELF (up) and LOL (down) contour planes for F^-–H^+–F^-, HO^-–H^+–OH^-, and H_3P–$H^+\cdots PH_3$. Labeled is the color scale of the values.

F. Discussions

From what has been discussed above, we can conclude that though two identical donors compete equally for H^+, it is not bound to form symmetric SSHBs. The results indicate that electronegativity of the central elements in L matters. More electronegative elements (group 17) are more willing to share protons and form SSHBs, whereas the donors with less electronegativity elements are more likely to form asymmetric typical HBs (groups 14 and 15). In addition, the patterns of HBs are different, although the central elements of donors belong to the same group. Because donors in HBs interact with H^+, we further calculated the basicity of different donors, and the bonding energies [Table I, $E = E(H^+–L) – E(H^+) – E(L)$] of H^+ with different bases (L) span over a wide range, from −76.28 to −420.60 kcal/mol. Based on the binding energy, it is clear that the strength of the Lewis base decreases in the order: NH_2^- > OH^- > PH_2^- > AsH_2^- > HS^- > SbH_2^- > F^- > HSe^- > Cl^- > HTe^- > Br^- > I^- for anion groups, and NH_3 > PH_3 > AsH_3 > SbH_3 > H_2O > H_2S > H_2Se > H_2Te > HF > HCl > HBr > HI for neutral groups. It is obvious that the types of HBs are related to the basicity, for both anion and neutral donors, stronger bases being more willing to form typical HBs while weaker bases being more likely to form SSHBs.

In addition, to further investigate the relationship between the strength of the HBs and electronegativity as well as basicity, Fig. 8 plots the binding energy of the HBs with BSSE correction [$E_b = E(L–H^+\cdots L) – E(L–H^+) – E(L)$] as a function of the electronegativity (χ)[75] of the central elements in L and the basicity of L (pK_b). There are good linear correlations between E_b and χ as well as pK_b, and $[F–H–F]^-$ has the strongest HB. For SSHB with halogen elements, E_b increases when the basicity increases. However, for typical HBs with stronger bases (OH^-, NH_2^-, and CH_3^-), E_b decreases with the increasing basicity, and that of H_3C^-–H^+–CH_3^- is fairly low.

As shown in Fig. S13, we further discussed compounds (L_1–H^+–L_2) formed by H^+ with two different electron donors L_1 and

TABLE I. Binding energy (E)[a] of H^+ with various bases in kcal/mol.

Bases	NH_2^-	OH^-	PH_2^-	AsH_2^-	HS^-	SbH_2^-
E	−426.09	−410.73	−409.08	−379.15	−359.68	−354.50
Bases	F^-	HSe^-	Cl^-	HTe^-	Br^-	I^-
E	−352.61	−347.45	−337.31	−335.00	−324.81	−314.40
Bases	NH_3	PH_3	AsH_3	SbH_3	H_2O	H_2S
E	−232.34	−216.04	−201.18	−187.47	−174.50	−145.12
Bases	H_2Se	H_2Te	HF	HCl	HBr	HI
E	−138.66	−134.47	−122.96	−72.49	−69.24	−68.40

[a]Binding energy of H^+–L is defined based on the calculation of $E = E(H^+–L) – E(H^+) – E(L)$.

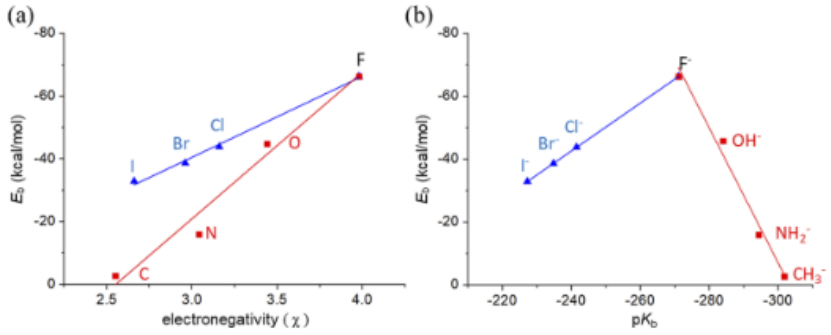

FIG. 8. Linear correlation plots between binding energy of L–H^+···L with BSSE correction [E_b = E(L–H^+···L) – E(L–H^+) – E(L)] and (a) electronegativity of the central elements of L (χ) as well as (b) the basicity of L (pK_b).

L_2 with gaps in basicity, and F^-–H^+···Cl^- and HO^-–H^+···Cl^- were selected. The different forces from the ligands on H^+ lead to asymmetric potential energy curves (Fig. S13b). Potential energy curves together with the optimized structures (Fig. S13a) show that H^+ strongly bond with more basic electron donors in each complex, suggesting typical HBs.

IV. CONCLUSIONS

In summary, we theoretically studied the properties of a series of compounds (L–H^+–L, L corresponds to donors containing group 14, 15, 16, and 17 elements) possessing similar structures to $[F–H–F]^-$, comprising H^+ and two identical electron donors. Though the forces coming from both sides are equal, they are not bound to form similar single-well HBs as $[F–H–F]^-$. Instead, both single- and double-well HBs exist. In addition, the impact of zero-point energy was explored. HO^-–H^+–OH^- changed from double-well HB with a rather low barrier to a single-well HB after considering the zero-point energy, while the patterns of the other studied compounds did not change. It was further found that the patterns of HBs were related to the electronegativity of donor elements. More electronegative elements are willing to share H^+ ions and form SSHBs. Meanwhile, the basicity of L also contributes to the patterns of HBs, and for both anion and neutral donors, weaker bases are more willing to form SSHBs while stronger ones are more willing to form typical HBs. There are good linear correlations between E_b and χ as well as pK_b. This work is expected to further deepen our understanding of hydrogen bonds.

SUPPLEMENTARY MATERIAL

See the supplementary material for geometric structure data, AdNDP, NCI, ELF, LOL, and energy decomposition analyses of complexes.

ACKNOWLEDGMENTS

This research was financially supported by the National Natural Science Foundation of China (Grant No. 21873001). The calculations were carried out at the High-Performance Computing Center of Anhui University. We gratefully acknowledge HZWTECH for providing computation facilities.

AUTHOR DECLARATIONS

Conflict of Interest

The authors have no conflicts to disclose.

Author Contributions

Wanwan Feng: Writing – original draft (lead). **Dan Li**: Writing – review & editing (lead). **Longjiu Cheng**: Conceptualization (lead); Supervision (lead).

DATA AVAILABILITY

The data that support the findings of this study are available from the corresponding authors upon reasonable request.

REFERENCES

[1] W. M. Latimer and W. H. Rodebush, J. Am. Chem. Soc. **42**, 1419 (1920).
[2] D. A. Decato, A. M. S. Riel, J. H. May, V. S. Bryantsev, and O. B. Berryman, Angew. Chem., Int. Ed. **60**, 3685 (2021).
[3] M. Hirahara, H. Nakano, K. Uchida, R. Yamamoto, and Y. Umemura, Inorg. Chem. **59**, 11273 (2020).
[4] M. Kumar and J. S. Francisco, J. Am. Chem. Soc. **142**, 6001 (2020).
[5] J. Yang, R. Dettori, J. P. F. Nunes, N. H. List, E. Biasin, M. Centurion, Z. Chen, A. A. Cordones, D. P. Deponte, T. F. Heinz, M. E. Kozina, K. Ledbetter, M.-F. Lin, A. M. Lindenberg, M. Mo, A. Nilsson, X. Shen, T. J. A. Wolf, D. Donadio, K. J. Gaffney, T. J. Martinez, and X. Wang, Nature **596**, 531 (2021).
[6] S. Sen and G. N. Patwari, ACS Omega **3**, 18518 (2018).
[7] P. Pandey, RSC Adv. **5**, 79661 (2015).
[8] M. Jabłoński, Chem. Phys. Lett. **477**, 374 (2009).
[9] B. C. Gibb, Nat. Chem. **12**, 665 (2020).
[10] J. M. Guevara-Vela, E. Romero-Montalvo, V. A. Mora Gómez, R. Chávez-Calvillo, M. García-Revilla, E. Francisco, Á. M. Pendás, and T. Rocha-Rinza, Phys. Chem. Chem. Phys. **18**, 19557 (2016).
[11] M. Saccone, M. Pfletscher, S. Kather, C. Wölper, C. Daniliuc, M. Mezger, and M. Giese, J. Mater. Chem. C **7**, 8643 (2019).
[12] C. C. Robertson, J. S. Wright, E. J. Carrington, R. N. Perutz, C. A. Hunter, and L. Brammer, Chem. Sci. **8**, 5392 (2017).
[13] K. Shin, I. L. Moudrakovski, C. I. Ratcliffe, and J. A. Ripmeester, Angew. Chem., Int. Ed. **56**, 6171 (2017).
[14] S. Saha, M. K. Mishra, C. M. Reddy, and G. R. Desiraju, Acc. Chem. Res. **51**, 2957 (2018).
[15] Y. Yu, T. Tyrikos-Ergas, Y. Zhu, G. Fittolani, V. Bordoni, A. Singhal, R. J. Fair, A. Grafmüller, P. H. Seeberger, and M. Delbianco, Angew. Chem., Int. Ed. **58**, 13127 (2019).